AD-A164 313 ACTA ARMAMENTARII (SELECTED ARTICLES)(U) FOREIGN TECHNOLOGY DIV WRIGHT-PATTERSON AFB OH Y ZHOU ET AL. 23 JAN 86 FTD-ID(RS)T-0907-85 1/1

UNCLASSIFIED F/G 21/8 NL

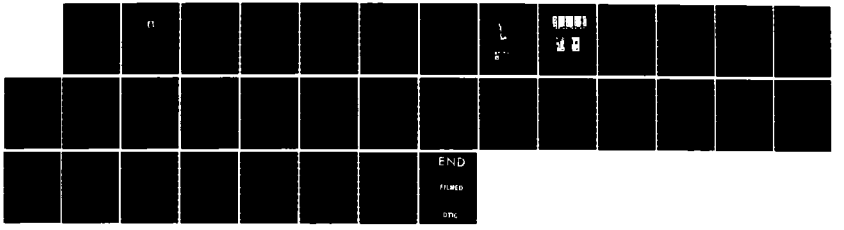

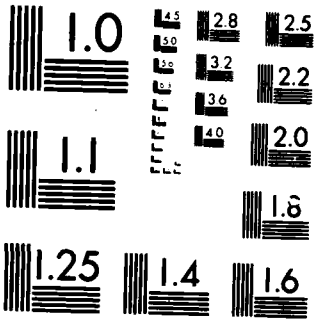

MICROCOPY RESOLUTION TEST CHART
NATIONAL BUREAU OF STANDARDS-1963-A

AD-A164 313

FTD-ID(RS)T-0907-85

FOREIGN TECHNOLOGY DIVISION

ACTA ARMAMENTARII

(SELECTED ARTICLES)

DTIC FILE COPY

DTIC ELECTE FEB 1 8 1986 S E D

Approved for public release;
distribution unlimited.

86 2 13 232

EDITED TRANSLATION

FTD-ID(RS)T-0907-85 23 Jan 86

MICROFICHE NR: FTD-86-C-001396

ACTA ARMAMENTARII (SELECTED ARTICLES)

English pages: 29

Source: Binggong Xuebao, Nr. 4, November, 1984, pp. 11-14; 40-49

Country of origin: China
Translated by: SCITRAN
F33657-84-D-0165
Requester: FTD/TQTA
Approved for public release; distribution unlimited.

THIS TRANSLATION IS A RENDITION OF THE ORIGINAL FOREIGN TEXT WITHOUT ANY ANALYTICAL OR EDITORIAL COMMENT. STATEMENTS OR THEORIES ADVOCATED OR IMPLIED ARE THOSE OF THE SOURCE AND DO NOT NECESSARILY REFLECT THE POSITION OR OPINION OF THE FOREIGN TECHNOLOGY DIVISION.

PREPARED BY:

TRANSLATION DIVISION
FOREIGN TECHNOLOGY DIVISION
WP-AFB, OHIO.

Table of Contents:

Foreign Technology, China, Translation

Accession For
NTIS GRA&I X
DTIC TAB
Unannounced
Justification
By
Distribution/
Availability Codes
Dist | Avail and/or Special
A-1

QUALITY INSPECTED 3

GRAPHICS DISCLAIMER

All figures, graphics, tables, equations, etc. merged into this translation were extracted from the best quality copy available.

Study of the Effect of Particle Density and Particle Size in a Gas-Solid Flow on the Drag Coefficient /11

Zhou Yanhuang, Sun Xingchang, Yin Hebao, Chen Xingquan and Li Guang

[Abstract] This paper shows the experimental results on the drag coefficient between the gas and solid phase within the range of Reynolds number Re = 10^2~10^6, void ε = 0.45~0.98 and equivalent particle diameter dp = 3~11mm. These results are also briefly analyzed and discussed.

A standard drag curve has already been given for the relationship between the drag coefficient of a spherical particle and Reynolds number[1,2]. (See Figure 6) S.L. Soo et al believed that this result could be applied to a dilute suspension[2]. In a packed bed loaded close to its maximum, people usually use the result obtained by Ergun[2,3]. In interior ballistics of a gun, during the initial combustion period, the ε of the particle bed is around 0.5. The equivalent diameter of the particle, dp, ranges from several to a dozen millimeters. E.B. Fisher[4], A.W. Horst[5], K.K. Kuo[6], F. Robbins and P.S. Gough[7] had studied this type of problem. Their joint conclusion was to continue using Ergun's results. There has been very little study in the drag coefficient in a scattered suspension with ε ranging from 0.45~0.98, which corresponds to the middle and late stage of combustion in interior ballistics. To date, we only find the equation proposed by K.K. Kuo which is based on the Ergun formula and Anderson formula[6]:

$$C_f = \begin{cases} 1.75 & (\varepsilon \leq \varepsilon_0) \\ 1.75\left(\frac{1-\varepsilon}{1-\varepsilon_0}\,\frac{\varepsilon_0}{\varepsilon}\right)^{n_{(\varepsilon)}} & (\varepsilon_0 < \varepsilon \leq \varepsilon_1) \\ 0.3 & (\varepsilon_1 < \varepsilon \leq 1.0) \end{cases} \qquad (1)$$

where C_f is the friction coefficient calculated based on the interfaced area. ε_0 and ε_1 are the porosity of critical fluidization and the maximum porosity, respectively. Usually, we choose $\varepsilon_1 = 0.98$. This equation has a very narrow application range; $0.003 < Re < 2000$.

Therefore, neither the standard drag curve (Figure 6) nor equation (1) can satisfactorily simulate the transport phenomenon of the particles in interior ballistics.

In order to verify and modify equation (1), to expand its applicable Reynolds number range, and to understand the deviation of the drag coefficient of the kind of particles of interest to us from Ergun's results, we did the following experiment in 1981.

Photographs of the experimental apparatus and some of the particles used in the experiment are shown in Figures 1 and 2. In order to measure the drag coefficients of loose particles at various porosities, ε, we prepared special specimens. Fine nylon lines were used to suspend particles according to specific distance and direction in the test section (See Figure 3). To the extent possible, we tried to make sure that the particles are uniformly distributed so that they are isotropical. The method used to test a packed bed is essentially the same as that employed by Fisher[4] and Horst[5]. The orientation of each particle is determined by the random process used for filling (See Figure 4).

During the experiment, the pressure drops across the bed at varying height were measured. In addition, parameters such as the apparent velocity were also obtained.

*Manuscript received on March 13, 1984 and revised manuscript received on June 25, 1984. This paper was presented at the Second Asian Fluid Dynamics Conference in October 1983.

/12

Figure 1. Experimental Apparatus

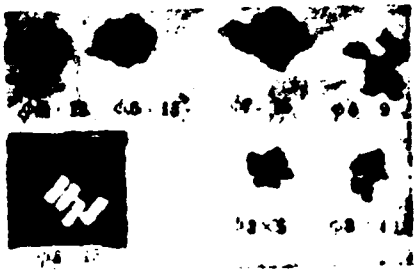

Figure 2. Some Particles Used in the Experiment

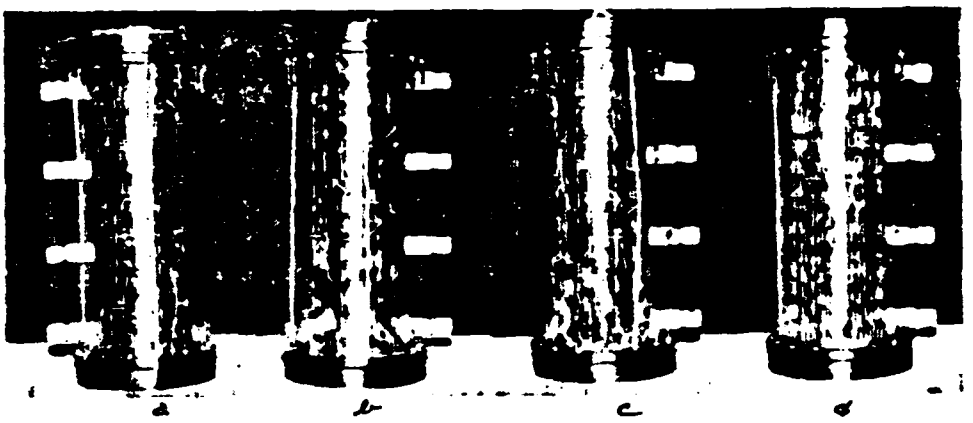

Figure 3. Specimens with Particles Spaced Uniformly

Figure 4. Particle Orientation Determined by Random Filling

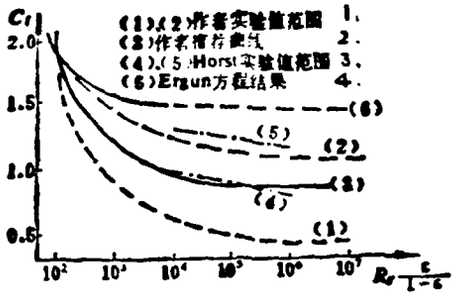

Figure 5. Friction Coefficient C_f vs. Re $\varepsilon/1-\varepsilon$

1. (1) and (2) show the range of experiment values obtained by the authors
2. (3) is the curve recommended by the authors
3. (4) and (5) are the range of Horst's experiment
4. (6) is the result of the Ergun equation

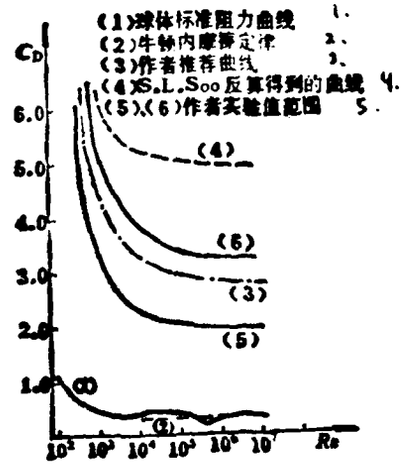

Figure 6. Drag Coefficient C_D vs Reynolds Number Re

1. (1) is stand drag curve for spheres
2. (2) is Newton's internal friction law
3. (3) is the curve recommended by the authors
4. (4) is the curve calculated by S.L. Soo
5. (5) and (6) show the range of experimental values obtained by the authors

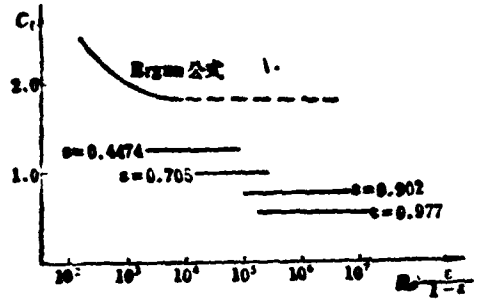

Figure 7. C_f vs Re $\varepsilon/1-\varepsilon$ at Various Porosities

1. Ergun equation

Hence, the friction coefficient can be determined by the following equation

$$C_f = \frac{\Delta p}{H} \Big/ \frac{1-\varepsilon}{\varepsilon^3} \frac{u_s^2 \rho_f}{d_p} \qquad (2)$$

where Δp is the pressure drop, H is the bed height, u_s is the apparent velocity of the gas, and ρ_f is the density of the gas. The drag coefficient C_D calculated based on the windward area of the particle is related to C_f as the following:

$$C_D = \frac{4}{3\varepsilon} C_f \qquad (3)$$

We measured various particles of 11 different geometric shapes at 6 ε values. After considering corrections for the nylon line and the mesh, we arrived at the following conclusions:

When $\varepsilon = 0.45$, based on our measured results and on the values reported in the literature[2,3,5], the relation between C_f and Re $\varepsilon/1-\varepsilon$ is just as the one shown in Figure 5. After certain transformation, the relation between C_D and Re is shown in Figure 6. At various ε, the relation between C_f and Re $\varepsilon/1-\varepsilon$ is shown in Figure 7. Based on these curves we can see that our results are 70% higher than those from the single sphere standard drag curve when the porosity $\varepsilon = 0.94\sim0.977$. At maximum packing, $\varepsilon=$ 0.45~0.47, the value of C_f we obtained is about 1.10, for less than 1.75. /14

Based on our measured results, the following relation is introduced:

$$C_t=\begin{cases} C_{fz} & (\varepsilon \leqslant \varepsilon_0) \\ C_{fz}\left(\dfrac{1-\varepsilon}{1-\varepsilon_0}\cdot\dfrac{\varepsilon_0}{\varepsilon}\right)^{4.21} & (\varepsilon_0 < \varepsilon \leqslant 0.97) \\ 0.45 & (0.97 < \varepsilon \leqslant 1) \end{cases} \tag{4}$$

where C_{fz} is defined by the following formula:

$$C_{fz}=\begin{cases} 0.31(\lg Re)^2-2.55\lg Re+6.4 & (Re<20000) \\ 1.10 & (Re\geqslant 20000) \end{cases} \tag{5}$$

The value obtained from this formula is far less than that from the Ergun equation. We believe that this discrepancy is due to particle size difference.

Due to the presence of particle clusters, the turbulent kinetic energy is excessively dissipated. The turbulence is damped. With particles of the same size, the smaller the porosity the smaller the gap between particles becomes. A large scale turbulence is being further divided and the larger the drag

coefficient becomes. In a suspension of the same porosity, the smaller the particle cluster size is, the smaller the average distance between particles is, and the larger the drag becomes. Thus, the difference between our results and those of Ergun can be fundamentally understood. Furthermore, in the extremely dilute case with $\varepsilon = 0.98$, we chose $C_f = 0.45$ instead of 0.30 as K.K. Kuo did in equation (2). This was based on the consideration that the particles we used were cylindrical. In addition, the authors believe that even when $\varepsilon \geqslant 0.98$ the interference among particles in the downstream flow field is unavoidable.

References

[1] Hinze J.O., Turbulence, Chapters 5-7, 1975.

[2] Soo S.L., Fluid Dynamics of Multiphase Systems, 1965.

[3] Ergun D., Chem. *Eng. Progr., 48, 89, 1952.

[4] Fisher E.B. and Trippe A.P., Mathematical Medel of Center Core Ignition in the 175mm Gun, Calspan Report, No. VQ-5163-D-2, March, 1974.

[5] Horst A.W., Journal of Ballistics, Vol. 14, No. 3, P. 836, 1980.

[6] Koo J.H. and Kuo K.K., Transient Combustion in Granular Propellant Beds, Part 1, AD-A 044998, 1977.

[7] Robbins F. and Gough P.S., An Experimental Determination of Flow Resistance in Packed Beds of Gun Propellent, Proceedings of the 15th JANAF Combustions Meeting, Sept., 1978.

[8] Krier H. and Summerfield M., Interior Ballistics of Guns, 1979.

A New Method of Rocket Nozzle Design /40

Qiu Guangshen

[Abstract] A new method of solid rocket nozzle design is introduced in this paper. This method, based on the theory of non-symmetric flow in a Lavol nozzle, is first focused on the reduction of aerodynamic misalignment and then on efficiency. It does not contradict other traditional methods. Instead, it supplements them. This design method will help reduce the scatter of impact of free flight rockets.

Table of Symbols

ϕ - potential function;

Φ - ϕ/α_t;

α_t - critical sound speed;

w - one-dimensional flow velocity coefficient;

h_i - coefficient of ϕ in flow equation as represented by dimensional flow parameters, when the subscripts i = 1, 2, 3 represent xx, rr, and rx, respectively;

f - small perturbation;

$(H_1)_R$ - partial derivative of H_1 with respect to R. The subscript may be x, θ or x, r. Two subscripts represent a second order partial derivative;

J_0, J_1 - zeroth and first order Bessel function;

β_1 - the first root of $J_1(\beta_n)=0$ which is chosen to be 1.841;

ρ_1 - local density;

T_1 - axial force per unit area at the outlet end;

r_1 - transverse cross-section radius;

$M\alpha$ - one-dimensional Mach number on the cross-section; a function of x alone;

dr_1/dx - slope of the bus line along ox direction, which is tg α in the linear portion;

r_t - radius of the nozzle throat;

R_t - radius of curvature of the throat;

L_t - lateral force at the throat;

k - specific heat ratio of the combustion gas;

$\gamma_{M\alpha}$ - the Planck-Myer expansion angle on a cross-section, which is a function of $M\alpha$;

w - mass of the propellant;

q_0 - total mass of the rocket.

Manuscript received on March 26, 1983, revision received on May 23, 1984.

1. Introduction /41

Because free flight rockets have poor density of impact, therefore, finding an easy and feasible method to improve density has been a major subject facing the free flight rocket technology. As far as rocket design is concerned, we should start with reducing the eccentricity of thrust. The primary component of thrust eccentricity is aerodynamic eccentricity. In recent years some foreign scholars conducted theoretical and experimental studies on the non-symmetric flow in a Lavol nozzle to provide the basis for new nozzle design. Normally, the principal objective of rocket design is to improve efficiency. The major

nozzle parameters, to some extent, are freely chosen by the designer. The new design method based on the above theory, however, is focused on the reduction of eccentricity, as well as on improvement of efficiency. It results in a nozzle whose theoretical aerodynamic eccentricity is zero. The nozzle will facilitate the improvement in the density of impact.

2. Brief Introduction to the Theory

The method introduced by A.G. Walters is to treat the non-symmetric three-dimensional flow in the nozzle based on one-dimensional flow with a small perturbation. In this work, the following basic assumptions are made. The expansion section of the nozzle is axial symmetric. The expansion semi-angle α is not too large. The principal lines are shown in Figure 2.1. The gas is an inviscid gas. The flow is steady, vortexless and isotropic. The perturbation is small and plane symmetric. Due to the fact that α is not too large, $tg\alpha$ and $\sin\alpha$ can be treated as small first order quantities. The calculation is accurate to the first order. The study is concentrated on the flow in the expansion section. We use a cylindrical coordinate where the ox-axis coincides with the axis of symmetry of the expansion section. The origin is located in the center of the throat.

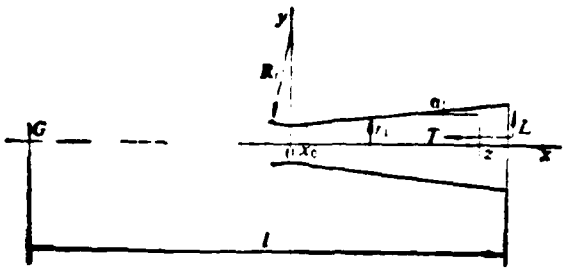

Figure 2.1 Nozzle Shape

First, the equation of the flow expressed by the potential function in the cylindrical coordinate is linearized. To this end, the following transformation is made

$$X = \int_0^x \frac{1}{r_1} \sqrt{\frac{h_1 h_2 + h_3^2}{h_1^2}}\, dx \tag{2.1}$$

$$R = \frac{r}{r_1} \tag{2.2}$$

Considering the fact that the flow near the throat is transonic, the expansion section of the nozzle is divided into two parts. The intersect of the curve and the straight line portion of the nozzle is the boundary; i.e., $x=x_0$. Corresponding to X, it is X_0. After neglecting small second and higher order terms, we get the following linear equation

$$\Phi_{XX} + \frac{\eta}{X}\Phi_X - \left(\Phi_{RR} + \frac{1}{R}\Phi_R + \frac{1}{R^2}\Phi_{\theta\theta}\right) = 0$$
$$\eta = \begin{cases} 1 & 0 < X \leqslant X_0 \\ 0 & X_0 < X \end{cases} \tag{2.3}$$

Multiply the above equation by cos θ and then integrate with respect to θ from 0-180°. /42

Let

$$H_1 = \int_0^{2\pi} \cos\theta \int_0^r \sqrt{\frac{w\phi_r}{w^2 + \frac{r}{r_1} f}}\, dr d\theta \tag{2.4}$$

After omitting second and higher order terms, we get the following equation

$$(H_1)_{xx} + \frac{\eta}{X}(H_1)_x - \left[(H_1)_{RR} + \frac{1}{R}(H_1)_R - \frac{H_1}{R^2}\right] = 0 \tag{2.5}$$

Its boundary condition is

$$(H_1)_R|_{R=1} = 0 \tag{A}$$

Its initial condition is

$$(H_1)|_{X=0} = F(R) \quad (H_1)_R|_{X=0} = 0 \tag{B}$$

By separation of variables equation (2.5) can be solved to get

$$H_1 = \sum_{n=1}^{\infty} A_n J_1(\beta_n R) I(\beta_n X) \tag{C}$$

F(R) is substituted into the equation for A_n to determine the A_n series. A_1 is the largest one and the rest decrease rapidly. Hence

$$H_1 = A_1 J_1(\beta_1 R) I_1(\beta_1 X) \tag{2.6}$$

$$I(\beta_1 X) = \begin{cases} J_0(\beta_1 X) & 0 < X \leq X_0 \\ J_0(\beta_1 X_0)\cos\beta_1(X - X_0) - J_1(\beta_1 X_0)\sin\beta_1(X - X_0) & X_0 < X \end{cases} \tag{2.7}$$

The relation between L and C_T is determined in the following.

The thrust is moved to the end surface of the nozzle exit along the line of action and then decomposed into two components T and L which are parallel and perpendicular to the axis. The moment of T around the center mass G of the entire rocket

(assuming G is on the axis) is TZ, which is denoted as C_T as shown in Figure 2.1. In view of the fact that the inner wall of the rocket engine is most frequently a body of rotation, when the nozzle and the combustion chamber are coaxial, L and C_T can be expressed in terms of the rate of change of the momentum and that of the moment of momentum of the gas at the end surface of the exit. Then, the following formula can be obtained.

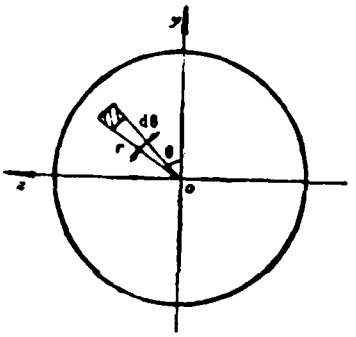

Figure 2.2 Top View of the End of the Nozzle Exit

$$L = -\int_0^{r_1}\int_0^{2\pi}(\rho_1\phi_{1x})\phi_1 r\,d\theta dr \tag{2.8}$$

$$C_T = \int_0^{r_1}\int_0^{2\pi} T_1 r^2\cos\theta\,d\theta dr \tag{2.9}$$

where the symbols relating to coordinates and angles are shown in Figure 2.2. Based on equations (2.8) and (2.9), by omitting second and higher terms, we can derive the following equation

$$L = -\frac{\dot{m}}{\pi r_1}a_1(H_1)_{x=r_1} - \frac{M_e^2-2}{M_e^2-1}\frac{C_T}{r_1}\frac{dr_1}{dx} \tag{2.10}$$

By taking a small element of the expansion section, we can get another formula

$$\frac{dC_T}{dx} + L - r_1 \frac{dr_1}{dx} \frac{dL}{dx} = 0 \qquad (2.11) \quad /43$$

Equations (2.10) and (2.11) are the fundamental equations to calculate the lateral force L and moment C_T.

In order to reduce the number of variables, we are using the following relative quantities

$$\bar{x} = \frac{x}{r_t} \quad \lambda = \frac{R_t}{r_t} \quad L^* = \frac{L}{L_n} \quad C_T^* = \frac{C_T}{r_t L_n} \qquad (A)$$

Equations (2.10) and (2.11) can be re-written in the following form

$$L^* = \frac{\gamma_t}{A_1 \gamma_1} (H_1)_{r=r_1} - \frac{Ma^2-2}{Ma^2-1} \frac{dr_1}{dx} \frac{r_t}{r_1} C_T^* \qquad (2.10')$$

$$\frac{dC_T^*}{dx} + \frac{L^*}{r_t} - \frac{r_1}{r_t} \frac{dr_1}{dx} \frac{dL^*}{dx} = 0 \qquad (2.11')$$

where

$$A_1 = -\frac{\pi r_t L_n}{m a_t} \qquad (B)$$

Because it is necessary to divide the expansion section into two in order to determine H_1, therefore, it is also required to divide it into two parts at x_0 (i.e., X_0) when we determine L* and C_T^*. In practice, the following re-arranged equations can be used in the calculation.

$$\bar{x}_0 = \frac{x_0}{r_t} = \lambda \sin \alpha$$

$$\frac{dr_1}{dx} = \begin{cases} \dfrac{\bar{x}}{\sqrt{\lambda^2 - \bar{x}^2}} & 0 < \bar{x} < \bar{x}_0 \\ \operatorname{tg} \alpha & \bar{x}_0 < \bar{x} \end{cases} \qquad (C)$$

$$\bar{r}_1 = \begin{cases} 1 + \lambda - \sqrt{\lambda^2 - \bar{x}^2} & 0 < \bar{x} < \bar{x}_0 \\ \bar{x} \operatorname{tg} \alpha + \left[1 - \dfrac{\lambda (1 - \cos \alpha)}{\cos \alpha} \right] & \bar{x}_0 < \bar{x} \end{cases}$$

Near the throat, i.e., at $\bar{x} \leqslant \bar{x}_0$,

$$X = 2\sqrt[4]{\frac{\lambda}{2(k+1)}}\sqrt{\bar{x}} \tag{D}$$

$$w = 1 + \bar{w}_1'\bar{x}$$

$$\bar{w}_1' = \left(\frac{dw}{d\bar{x}}\right)_{x=x_1} = \sqrt{\frac{1}{\lambda(k+1)}}$$

The relation between the one-dimensional flow Mα and the velocity coefficient w is

$$M^2 = \frac{2w^2}{k+1-(k-1)w^2} \tag{E}$$

Far away from the throat, i.e., $\bar{x}_0 < \bar{x}$

$$\frac{dX}{dx} = \frac{1}{r_1}\frac{1}{\sqrt{Ma^2-1}}$$

$$\frac{dM}{dx} = \frac{2Ma\Gamma}{Ma^2-1}\frac{dr_1}{dx}\frac{1}{r_1} \tag{F}$$

From equations (2.10') and (2.11') we get

/44

$$\frac{dC_T^*}{dx} = \begin{cases} E_4\frac{dr_1}{dx}C_T^* - E_3\left[J_0(\beta_1 X) + \frac{\beta_1 J_1(\beta_1 X)}{\sqrt{Ma^2-1}}\frac{dr_1}{dx}\right] & 0 < \bar{x} \leqslant \bar{x}_0 \\ E_4\frac{dr_1}{dx}C_T^* - E_3\left[I_1 - I_2\frac{1}{\sqrt{M_0^2-1}}\frac{dr_1}{dx}\right] & \bar{x}_0 < \bar{x} \end{cases}$$

$$L^* = \begin{cases} -E_3 J_0(\beta_1 X) & 0 < \bar{x} \leqslant \bar{x}_0 \\ -E_3 I_1 - E_4 C_T^*\frac{dr_1}{dx} & \bar{x}_0 < \bar{x} \end{cases} \tag{A}$$

$$E_3 = \left(\frac{k+1}{2\Gamma}\right)^{\frac{k+1}{4(k-1)}}\sqrt{Ma}$$

$$E_4 = E_3\frac{Ma^2-2}{Ma^2-1}$$

$$\Gamma = 1 + \frac{k-1}{2}Ma^2$$

$$I_1 = J_0(\beta_1 X_0)\cos\beta_1(X-X_0) - J_1(\beta_1 X_0)\sin\beta_1(X-X_0)$$

$$I_2 = -\beta_1 J_0(\beta_1 X_0)\sin\beta_1(X-X_0) - \beta_1 J_1(\beta_1 X_0)\cos\beta_1(X-X_0)$$

Based on the above equations, we can find the curves showing L and C_T vs. x, as shown in Figure 2.3. L and C_T oscillate with increasing x. The amplitude of L is decreasing while that of C_T is increasing. The phase difference between the two is approximately $2/3\pi$.

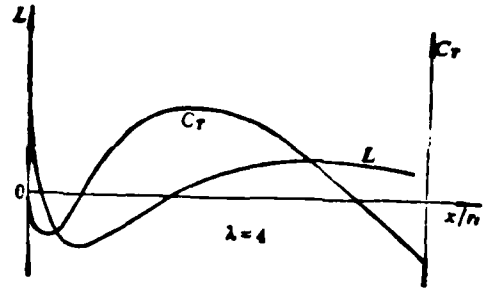

Figure 2.3 Lateral Force and Moment with Varying Expansion Section Length

We verified this theory experimentally and proved that it is accurate. For instance, a comparison is made with respect to the x/r_t at L=0. The result is shown in Table 2.1.

Table 2.1 Comparison of Experimental and Theoretical Values

n	1. [illegible]	2. [illegible]	3. [illegible]
2	10.16	10.21	0.5%
3	16.17	17.21	6.4%

1. experimental value
2. theoretical value
3. relative error

The paper by A.G. Walters introduced the experimental results and arrived at the same conclusions.

From Figure 2.1 we can see that, if we assume the distance from the end of the nozzle outlet to the center of mass G is 1, then the moment of thrust around G - the thrust eccentricity moment can be calculated based on the following formula

$$M_c = Ll + Tz = Ll + C_T \qquad (2.12) \quad /45$$

From the correlations in the L-x and C_T-x curves we can see that there is a suitable x, which can be chosen as the length of the expansion section, to realize M_c=0. The condition is

$$\frac{L}{C_T} = -\frac{1}{l} \quad \text{or} \quad \frac{L^*}{C_T^*} = -\frac{1}{l} \qquad (2.13)$$

In reality, L and C_T are not only related to x, but also to other parameters of the expansion section such as α and R_t, as well as to the value of k of the combustion gas. Therefore, we can choose a set of appropriate parameters to meet the requirement M_c =0. For convenience, we suggest that this type of nozzle whose theoretical thrust eccentricity moment is zero should be called the zero eccentricity moment nozzle. The results of the flight experiment were also introduced in A.G. Walters' paper. The presence of this type of nozzle was proven.

3. Nozzle Design

The principal lines shown in Figure 3.1 are frequently used in free flight rockets. The advantage is ease of fabrication. However, irregular aerodynamic misalignment may result, which will hurt the density of impact. Because of the sharp edge at

the front and rear end of the throat and at the intersect of the contracting cone and expansion cone, it is easy to be eroded by the combustion gas to form irregular arcs, leading to irregular changes of L and C_T. Hence, there is a need to use a circular arc at the interface to eliminate erosion. The principal lines of the nozzle used in the theoretical derivation are shown in Figure 3.1b or Figure 2.1. There is no cylindrical section at the throat which obviously does not favor mass production. It is more appropriate to change to the nozzle line (mainly at the throat and its neighborhood) shown in Figure 3.1c. The use of the R_t' arc as a transition step will favor the reduction of the flow perturbation at the throat and the improvement of the homogeneity of the flow at the throat cross-section. The expansion section of this type of nozzle has five parameters: r_t, r_e, R_t, α and x. As far as the principal line is concerned, r_t is a constant. Only three of the remaining four are independent. They satisfy the following relation:

$$\xi = \frac{r_e}{r_t} = (\bar{x} - \lambda \sin\alpha)\operatorname{tg}\alpha + \lambda(1 - \cos\alpha) + 1 \qquad \text{(A)}$$

In order to link to the conventional nozzle design methods, we choose ξ, λ and α as independent variables.

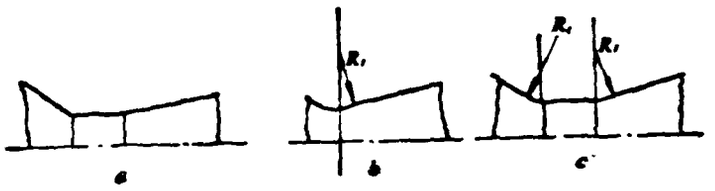

Figure 3.1 Shape Near the Throat

In the initial stage of rocket design, only a rough shape of the nozzle must be determined. In addition, if the condition M_c =0 is used, the $\bar{\iota}$ in equation (2.13) is still an unknown or is not precisely known. Thus, the design work cannot proceed. In view of the fact that for most free flight rockets $\bar{\iota}$ is a large number and the calculation shows that the value of C_T is very small, the requirement M_c=0 will demand that L.1 and C_T are equal but opposite in sign. Thus, we can determine that the point which satisfies this condition must near L=0. Hence, nozzle design can be carried out in two steps; preliminary design and accuracy connection.

3.1 Preliminary Design

In equation (2.10), there is a factor dr_1/dx, which is tgα, in the second term on the right. It is a small quantity. After neglecting this term, based on the fact that L = 0, we get

$$(H_1)_{r=r_1}=0 \qquad (B)$$

Obviously, we will not design a nozzle with $x<x_0$. Therefore, we must use the second type of solution for $I(\beta, X)$. Because $A_1 J_1(\beta_1) \neq 0$, then /46

$$J_0(\beta_1 X_0)\cos\beta_1(X-X_0)-J_1(\beta_1 X_0)\sin\beta_1(X-X_0)=0 \tag{A}$$

The solution obtained is

$$X=X_0+\frac{1}{\beta_1}\left[n\pi+\mathrm{tg}^{-1}\frac{J_0(\beta_1 X_0)}{J_1(\beta_1 X_0)}\right] \tag{3.1}$$

In the formula to calculate X, there are h_1, h_2 and h_3. After neglecting second and higher order small terms, we can derive the following

$$X=X_0+\frac{1}{\frac{dr_1}{dX}}[\nu(Ma)-\nu(Ma_0)] \tag{3.2}$$

After combining (3.1) and (3.2) we get

$$\nu(Ma)=\nu(Ma_0)+\frac{2}{\beta_1}\frac{dr_1}{dx}\left[n\pi+\mathrm{tg}^{-1}\frac{J_0(\beta_1 X_0)}{J_1(\beta_1 X_0)}\right] \tag{3.3}$$

$$\nu(Ma)=\sqrt{\frac{k+1}{k-1}}\,\mathrm{tg}^{-1}\sqrt{\frac{k-1}{k+1}(Ma^2-1)}-\mathrm{tg}^{-1}\sqrt{Ma^2-1} \tag{3.4}$$

The initial values in equations (3.1) through (3.4) can be calculated based on the following formulas:

$$\begin{cases} \bar{x}_0=\lambda\sin\alpha \\ \bar{w}_0'=\left(\frac{d\bar{w}}{d\bar{x}}\right)_0=\sqrt{\frac{1}{(k+1)\lambda}} \\ w_0=1+\bar{w}_0'\bar{x}_0 \\ X_0=\frac{2\bar{x}_0}{(k+1)\bar{w}_0'}\left(1-\frac{k}{9}\bar{x}_0\bar{w}_0'\right) \\ Ma_0=\sqrt{\frac{2w_0^2}{(k+1)-(k-1)w_0^2}} \end{cases} \tag{3.5}$$

Based on equations (3.2) to (3.5), we can get a family of ξ-α curves using λ as the parameter at fixed k and n, as shown in Figure 3.2. Any point on the curve represents a nozzle parameter. This parameter satisfies the condition

$$(H_1)_{r=r_1}=0, \text{ i.e. } L\approx 0$$

Based on Figure 3.2, we can see that there are many nozzle parameters satisfying the above condition. Selecting a set of values from these combinations of parameters must also be based on other conditions, such as improved efficiency and structural requirements. The design of a zero thrust eccentricity nozzle is to introduce a constraint of nozzle parameters to reduce the aerodynamic eccentricity moment. It does not confuse the conventional design methods.

Due to the fact that $(H_1)_{r=r_1}=0$ can only make the first term on the right of the L formula zero, therefore, the lateral force of the nozzle from Figure 3.2 should be

$$L_1=-\frac{Ma^2-2}{Ma^2-1}\frac{C_r}{r_1}\frac{dr_1}{dx}\approx 0 \qquad \text{(A)}$$

Using the value of x corresponding to L=0 as a reference point, because $L_1<0$, therefore, the point corresponding to L_1 must be on its left. Please refer to Table 3.1 for the values of $\bar{x}$ listed.

If $M_c=0$ is the condition, then L and C_T must have opposite signs. Based on the correlation between L-x and C_T-x curves we can see that this point must also be located to the left of the reference point (corresponding to L=0). Hence, the nozzle prototype determined by Figure 3.2 will not be far off from the /47 zero thrust eccentricity nozzle.

Both equations (2.10) and (2.11) are obtained by the same perturbation factor. In reality, there are numerous factors capable of producing perturbance. Furthermore, they are complex. Considering the small perturbation assumption, the effect of various factors is independent. The combined effect is the sum of all effects. Therefore, as long as the perturbation satisfies the initial condition, because $M_{ci}=0$, then $\Sigma M_{ci}=0$. Hence, the theoretical value of the aerodynamic eccentricity moment of the nozzle under various perturbations is still zero.

3.2 Accuracy Correction

The prototype nozzle obtained from preliminary design does not satisfy the condition $M_c=0$. As the design work proceeds, various data are obtained and become more accurate. After the specific conditions are established, the formulas mentioned above are used to calculate L^*, C_T^*, and C_T^*/L^*. The set of parameters chosen based on the condition $C_T^*/L^*=1/\bar{\tau}$ with equation (2.13) are the zero eccentric thrust moment parameters. Prototype parameters do not agree with this fact. We must rationally modify it to satisfy $M_c=0$.

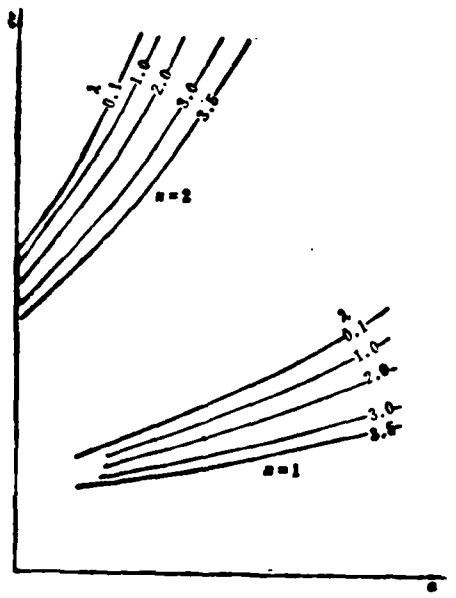

Figure 3.2 Nozzle Expansion Ratio Vs. Semi-angle of Expansion

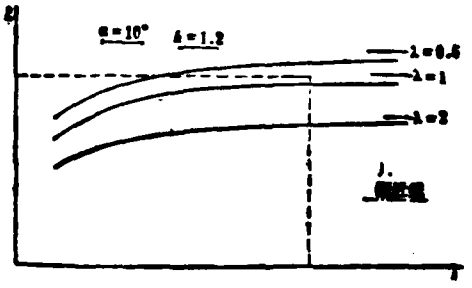

Figure 3.3 Nozzle Expansion Ratio Vs. 1

1. asymptotic curve

Table 3.1 Comparison of Zero Points

$\alpha = 10^{\circ}$ $k = 1.2$

L \ λ	0.5	1.0	2.0
0	5.895	5.585	4.96
L_1	5.29	5.10	4.66

For convenience, we can refer to a family of curves or a data table. Figure 3.3 shows a family of ξ-$\bar{l}$ curves. They are calculated from the C_T^*/L^*-x curve. The variables are α, λ and k. If ξ of the nozzle remains unchanged, $\bar{l}$ is known (expressed in terms of $\bar{l}_R$), and both intersect at A, other parameters at A can be determined from the curve. The prototype nozzle can then be adjusted based on these parameters.

Due to the fact that the theoretical and calculated results are very close, especially the difference between the nozzle line and its actual shape in deriving the formula, the corrected nozzle must still be experimentally verified. Because the lateral force and moment are not too large, their influencing factors are incidental. Therefore, the magnitude and direction of the lateral force are random. This special feature must be considered in arranging the experiment.

3.3 Determination of l_R

The method mentioned above is essentially using the baseline of the nozzle to control the line of thrust action. Once the nozzle parameters are determined, the intersect between the line of thrust action and the axis of symmetry is fired. If the intersect coincides with the center of mass of the rocket G, then $M_c=0$. During the active flight period, however, the charge of the rocket is continuously consumed and exhausted. The center of mass G is not fixed. It usually moves toward the head. /48 Therefore, it is not possible to keep $M_c\equiv 0$. Hence, it is necessary to determine an appropriate l value to satisfy the design requirements for zero eccentric thrust moment nozzles.

Figure 3.4 shows the relevant symbols. G_∞ is the center of mass of the propellant. l_∞ is considered not to vary with time. G_0 and G_k are the center of mass of the rocket before ignition and after the propellant is combusted, respectively. G_k is chosen to be located between G_0 and G_R. In addition, it meets the condition that the misalignment angle of the total thrust is zero.

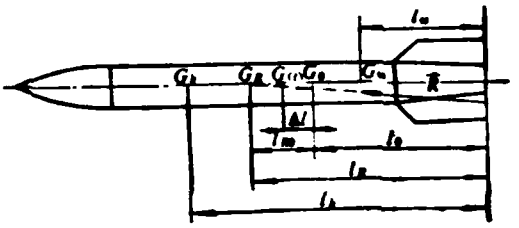

Figure 3.4 Centers of Mass and Relevant Symbols

i.e.

$$\psi_{M_c'} = 0 \tag{A}$$

Let us assume that the instantaneous center of mass G(t) is at a distance Δl from G_0 and G_R is at a distance l_{R_0} from G_0. Based on formulas to calculate $\psi_{M'_c}$ and M'_c, the following equation can be obtained by using the above condition

$$l_{R_0} = \frac{\int_{t_0}^{t} \Delta l \psi_{v_0}^{\circ}(x_m, u)\,dt}{\int_{t_0}^{t} \psi_{v_0}^{\circ}(x_m, u)\,dt} \tag{3.6}$$

where Δl is calculated according to the following approximation

$$\Delta l = \frac{l_0 - l_R}{\theta_0 - \frac{\omega}{\tau} t} \frac{\omega}{\tau} t \tag{3.7}$$

The upper limit of integration in equation (3.6) can be selected in two ways. One is to choose 0.7~0.8 of the time corresponding to the critical arc length. Or, we may choose τ. In order to use the value of exterior ballistics, the former upper time limit is selected. l_{R_0} can also be calculated by the following

approximation

$$l_{R_0}=\frac{\sum_{k=1}^{n}\frac{1}{2}(\Delta l_k-\Delta l_{k-1})\psi_{\tau_0}^{*}(u_k,\ u_{k-1})(t_k-t_{k-1})}{\sum_{k=1}^{n}\psi_{\tau_0}^{*}(u_k,\ u_{k-1})(t_k-t_{k-1})} \tag{3.6'}$$

where t_k is the time corresponding to u_k.

$$l_R=l_0+l_{R_0} \tag{3.8}$$

The curve in Figure 3.5 is obtained based on equation (3.6'). We can see that l_{R_0} varies very slowly beyond u=4.5.

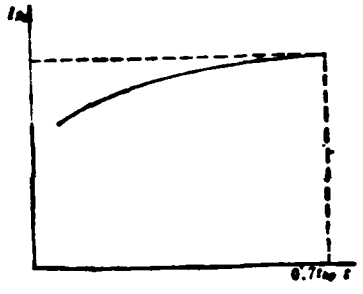

Figure 3.5 l_{R_0} Vs. Time

References /49

[1] Walters A.G., Non-Symmetric Flow in Laval type Nozzles, Phil. trans. Roy. Soc. London 1972, vol A, 273, No. 1232.

[2] Darwell H.M., Trubridge G.F.P., Design of Rocket Nozzles to Gas Misalignment, J. of Spacecraft and Rockets, vol 5, No. 1, January 1968.

[3] Xu Mingyou: ((Exterior Ballistics of Rockets)), Defense Publishing Co, 1980.

END

FILMED

4-86

DTIC